UNIVERSIDAD DE CONCEPCIÓN

Centro de Investigación en Ingeniería Matemática (CI^{2}MA)

Polynomial viscosity methods for multispecies kinematic flow models

Raimund Bürger, Pep Mulet,
Lihki Rubio

PREPRINT 2015-29

SERIE DE PRE-PUBLICACIONES

POLYNOMIAL VISCOSITY METHODS FOR MULTISPECIES KINEMATIC FLOW MODELS

RAIMUND BÜRGER[A], PEP MULET[B], AND LIHKI RUBIO[C]

Abstract. Multispecies kinematic flow models are defined by systems of strongly coupled, nonlinear first-order conservation laws. They arise in various applications including sedimentation of a polydisperse suspensions and multiclass vehicular traffic. Their numerical approximation is a challenge since the eigenvalues and eigenvectors of the corresponding flux Jacobian matrix have no closed algebraic form. It is demostrated that a recently introduced class of fast first-order finite volume solvers, called PVM (polynomial viscosity matrix) methods [M.J. Castro Díaz and E. Fernández-Nieto, SIAM J Sci Comput 34 (2012), A2173–A2196] can be adapted to multispecies kinematic flows. PVM methods have the advantage that they only need some information about the eigenvalues of the flux Jacobian, and no spectral decomposition of a Roe matrix is needed. In fact, the so-called interlacing property (of eigenvalues with known velocity functions), which holds for several important multispecies kinematic flow models, provides sufficient information for the implementation of PVM methods. Several variants of PVM methods (differing in polynomial degree and the underlying quadrature formula to approximate the Roe matrix) are compared by numerical experiments. It turns out that PVM methods are competitive in accuracy and efficiency with several existing methods, including the HLL method and a spectral WENO scheme that is based on the same interlacing property.

1. Introduction

1.1. **Scope.** This work concerns high-resolution numerical schemes for systems of conservation laws that arise as one-dimensional multiclass kinematic flow models describing the flow of one disperse substance through a continuous phase. In many cases, the disperse substance consists of small particles of different species that differ in size or density, segregate, and create areas of different composition. Such models include a model of polydisperse sedimentation of solid-liquid suspensions with solid particles of different sizes, and also certain continuum approximations of traffic flow of vehicles on a highway with drivers having different preferential velocities.

These models describe the spatio-temporal evolution of local concentrations $\phi_i = \phi_i(x,t)$ of species i through the continuity equations of the N species $\partial_t \phi_i + \partial_x(\phi_i v_i) = 0$, $i = 1,\dots,N$, where t is time, x is the spatial variable, and the velocities $v_1,\dots,v_N$ are assumed to be given functions of the vector $\Phi := \Phi(x,t) := (\phi_1(x,t),\dots,\phi_N(x,t))^{\mathrm{T}}$. This yields nonlinear, strongly

Date: August 15, 2015.

Key words and phrases. Polynomial viscosity matrix, Roe matrix, systems of conervation laws, multispecies kinematic flow model, polydisperse sedimentation, multiclass traffic model.

[A]CI^{2}MA and Departamento de Ingeniería Matemática, Facultad de Ciencias Físicas y Matemáticas, Universidad de Concepción, Casilla 160-C, Concepción, Chile. E-Mail: rburger@ing-mat.udec.cl.

[B]Departament de Matemàtica Aplicada, Universitat de València, Av. Dr. Moliner 50, E-46100 Burjassot, Spain. E-Mail: mulet@uv.es.

[C]CI^{2}MA and Departamento de Ingeniería Matemática, Facultad de Ciencias Físicas y Matemáticas, Universidad de Concepción, Casilla 160-C, Concepción, Chile. E-Mail: lrubio@ing-mat.udec.cl.

coupled systems of conservation laws of the type

$$\partial_t \Phi + \partial_x \boldsymbol{f}(\Phi) = 0, \quad \boldsymbol{f}(\Phi) := \big(f_1(\Phi), \ldots, f_N(\Phi)\big)^{\mathrm{T}}, \tag{1.1}$$

$$f_i(\Phi) := \phi_i v_i(\Phi), \quad i = 1, \ldots, N, \tag{1.2}$$

supplied with suitable initial or boundary conditions.

Numerical methods for hyperbolic conservation laws need some sort of upwinding to be stable. For scalar conservation laws, upwinding is a well-established issue. For hyperbolic systems of conservation laws, there are at least two alternatives for upwinding: one may locally project the solution information onto characteristic fields, and then apply the usual techniques for scalar conservation laws to each field; or alternatively, one can use flux-splitting methods with a high amount of numerical viscosity. The first alternative, that yields characteristic-wise numerical schemes, gives better resolution than the second, since the amount of numerical viscosity is much smaller for the latter. The prototype of this kind of methods is Roe's method [1] (see also [2]), for which the first-order numerical flux, specified here for two adjacent states Φ_{L} and Φ_{R} to left and right of a cell boundary, is given by

$$\hat{\boldsymbol{f}}(\Phi_{\mathrm{L}}, \Phi_{\mathrm{R}}) = \frac{1}{2}\Big(\boldsymbol{f}(\Phi_{\mathrm{L}}) + \boldsymbol{f}(\Phi_{\mathrm{R}}) - \big|\boldsymbol{A}(\Phi_{\mathrm{L}}, \Phi_{\mathrm{R}})\big|(\Phi_{\mathrm{R}} - \Phi_{\mathrm{L}})\Big), \tag{1.3}$$

where $\boldsymbol{A}(\Phi_{\mathrm{L}}, \Phi_{\mathrm{R}})$ is a Roe matrix (related to the flux Jacobian $\mathcal{J}_{\boldsymbol{f}} = (\partial f_i/\partial \phi_j)_{1\le i,j\le N}$) for the flux $\boldsymbol{f}$ and $|\boldsymbol{A}| \in \mathbb{R}^{N\times N}$ denotes a real diagonalizable matrix that is computed through the eigenvectors and eigenvalues of $\boldsymbol{A}$ (not to be confused with the matrix of absolute values of the entries of $\boldsymbol{A}$). On the other hand, the second alternative, which gives rise to component-wise schemes, tends to yield faster methods. Thus, the relative efficiency of one alternative with respect to the other is problem dependent. Roughly speaking, if the characteristic information (eigenstructure of the flux Jacobian) is available in closed form, then the first alternative tends to be more efficient; otherwise, if the characteristic information requires a high computational effort, then the second may turn out to be more efficient. Some kinematic flow models (1.1), (1.2) have flux Jacobians of arbitrary size N, without readily available characteristic information, but they can be proved to be hyperbolic by other means [3]. For some of these models characteristic-wise schemes are more efficient than some component-wise schemes [3, 4], essentially because the component-wise schemes used in the comparison prescribe a global numerical viscosity that tends to smear out relevant singularities of the solution.

The purpose of this paper is to explore a class of numerical methods, so-called Polynomial Viscosity Matrix (PVM) methods [5], whose aim is to mimic Roe's method without using the characteristic information. These methods approximate $|\boldsymbol{A}|$ by $P(\boldsymbol{A})$ for some suitably defined polynomial P that approximates the function $x \mapsto |x|$ in some interval containing the eigenvalues of $\boldsymbol{A}$. The main difficulties that are encountered in this work are the unavailability of a Roe matrix, at least in closed form, and that the characteristic fields may not be genuinely nonlinear (for scalar conservation laws this corresponds to fluxes with inflection points).

1.2. **Related work.** The PVM methods were studied in [6]. That work includes numerous applications of PVM methods to hyperbolic systems of conservation laws with source terms or nonconservative products. These methods have the advantage that they only need partial information on the eigenvalues of the system, and no spectral decomposition of a Roe matrix is required. We therefore propose to apply PVM methods to multispecies kinematic flow models [7], which give rise to systems of conservation laws (1.1), (1.2) that are constructed in a systematic way but for which the spectral information of $\mathcal{J}_{\boldsymbol{f}}(\Phi)$ is, in general, not available in closed form. The best-known model of this type is the multi-class Lighthill-Whitham-Richards (MCLWR) kinematic traffic model, which extends

the well-known Lighthill-Whitham-Richards (LWR) model [8, 9] to vehicles with drivers having different preferential velocities, and which was proposed by Benzoni-Gavage and Colombo [10] and Wong and Wong [11]. A very similar model, posed with zero-flux boundary condidions, describes the settling of emulsions [12]. The velocity functions v_i in these applications have an algebraically simple structure in the sense that the resulting flux Jacobian matrix $\mathcal{J}_{\boldsymbol{f}}(\Phi)$ is a rank-m perturbation of a diagonal matrix with $m = 1$. More involved velocity functions, for which the corresponding rank is $m \geq 2$, arise in models of sedimentation of polydisperse suspensions, see [3, 13] and the references cited in these papers.

1.3. **Outline of this paper.** The remainder of this paper is organized as follows. In Section 2 we describe the kinematic flow models under consideration. In Section 2.1 we first recall the interlacing property (of the eigenvalues of the flux Jacobian with known velocity functions and extremal bounds) common to the specific models considered herein. Then we outline the models of polydisperse sedimentation (Section 2.2) and multiclass vehicular traffic (Section 2.3). In Section 3 we expound PVM methods, starting with a description of the basic semi-discrete and fully discrete finite volume discretizations and recalling the role of a Roe matrix in that context (Section 3.1). Next, we introduce in Section 3.2 the concept of a polynomial viscosity matrix (PVM) that may replace a Roe matrix when the computational cost of obtaining the latter is unacceptably high. There are many different plausible choices of the polynomial P that underlies a specific PVM method. Some common choices are mentioned in Section 3.3. Specific issues about the implementation of PVM methods for kinematic flow models related to the general unavailability of Roe matrices and bounding eigenvalues are discussed in Section 3.4. Finally, we specify in Section 3.5 the MUSCL technique of variable extrapolation in combination with Heun's method of time integration to produce PVM methods of formal second order accuracy. In Section 4 we perform some simulations with the purpose of showing that the decision-making process that has been carried out leads to robust and efficient numerical schemes for the approximate solution of the considered kinematic models. Finally, in Section 5 we draw some conclusions and discuss some open issues.

2. Multispecies kinematic flow models

2.1. **Interlacing property.** Kinematic flow models are given by systems of conservation laws (1.1) with fluxes given by (1.2) for sufficiently smooth functions v_i. However, in most applications these functions do not depend individually on each of the densities $\phi_1, \ldots, \phi_N$ but rather on a small number $m \ll N$ of functions $p_1, \ldots, p_m$ of $\phi_1, \ldots, \phi_N$, i.e.,

$$v_i = v_i(p_1, \ldots, p_m), \quad p_l = p_l(\phi_1, \ldots, \phi_N), \quad i = 1, \ldots, N, \quad l = 1, \ldots, m, \quad m \ll N.$$

Under this assumption the Jacobian $\mathcal{J}_{\boldsymbol{f}} = \mathcal{J}_{\boldsymbol{f}}(\Phi)$ is a matrix of the form

$$\mathcal{J}_{\boldsymbol{f}} = \boldsymbol{D} + \boldsymbol{B}\boldsymbol{C}^{\mathrm{T}}, \quad \boldsymbol{D} := \operatorname{diag}(v_1, \ldots, v_N), \tag{2.1}$$

$$\boldsymbol{B} := (b_{il}) = \left(\phi_i \frac{\partial v_i}{\partial p_l}\right), \quad \boldsymbol{C} := (c_{ij}) = \left(\frac{\partial p_l}{\partial \phi_j}\right), \quad 1 \leq i, j \leq N, \quad 1 \leq l \leq m. \tag{2.2}$$

The following theorem is proved in [14]. It is applied in [3,4,15] to prove hyperbolicity of selected multispecies kinematic flow models and for the construction of spectral numerical schemes.

Theorem 2.1 (Secular Equation [14,15])**.** *Assume that $\boldsymbol{D}$ is a diagonal matrix as given by* (2.1) *with $v_i > v_j$ for $i < j$ and that $\boldsymbol{C}$ and $\boldsymbol{B}$ have the formats specified in* (2.2)*. Let $\lambda \neq v_i$ for*

$i = 1, 2, \ldots, N$. Then λ is an eigenvalue of $\boldsymbol{D} + \boldsymbol{B}\boldsymbol{C}^{\mathrm{T}}$ if and only if

$$R(\lambda) := \det M_\lambda = 1 + \sum_{i=1}^{N} \frac{\gamma_i}{v_i - \lambda} = 0.$$

The coefficients $\gamma_1, \ldots, \gamma_N$ are given by the following expression, where $I := \{i_1 < \cdots < i_k\} \in S_k^N$ and $J := \{j_1 < \cdots < j_l\} \in S_l^m$ are index sets:

$$\gamma_i = \sum_{r=1}^{\min N, M} \sum_{i \in I \in S_r^N, J \in S_r^m} \frac{\det \boldsymbol{C}^{I,J} \det \boldsymbol{B}^{I,J}}{\prod_{l \in I, l \neq i}(v_l - v_i)}.$$

Corollary 2.1 (Interlacing property [3])**.** *With the notation of Theorem 2.1, assume that $\gamma_i \gamma_j > 0$ for $i, j = 1, \ldots, N$. Then $\boldsymbol{D} + \boldsymbol{B}\boldsymbol{C}^{\mathrm{T}}$ is diagonalizable with real eigenvalues $\lambda_1, \ldots, \lambda_N$. If $\gamma_1, \ldots, \gamma_N < 0$, the interlacing property*

$$M_1 := v_N + \gamma_1 + \cdots + \gamma_N < \lambda_N < v_N < \lambda_{N-1} < \cdots < \lambda_1 < v_1 \tag{2.3}$$

holds, while for $\gamma_1, \ldots, \gamma_N > 0$, the following analogous property holds:

$$v_N < \lambda_N < v_{N-1} < \lambda_{N-1} < \cdots < v_1 < \lambda_1 < M_2 := v_1 + \gamma_1 + \cdots + \gamma_N$$

2.2. **Polydisperse sedimentation models.** Polydisperse suspensions consist of small solid particles that belong to a number N of species that differ in size, and which are dispersed in a viscous fluid. The sizes are assumed to be ordered as $D_1 > D_2 > \cdots > D_N$. The sedimentation of such a mixture of given initial concentration $\Phi_0(x)$ in a column of depth L can be then described by (1.1), (1.2), where ϕ_i denotes the local volume fraction of particle species i having diameter D_i, supplied with the initial condition

$$\Phi(x, 0) = \Phi_0(x), \quad x \in (0, L) \tag{2.4}$$

and zero-flux boundary conditions

$$\boldsymbol{f}|_{x=0} = \boldsymbol{f}|_{x=L} = \boldsymbol{0}, \quad t > 0. \tag{2.5}$$

A widely used velocity model for polydisperse sedimentation is the Masliyah-Lockett-Bassoon (MLB) model [16, 17]. This model arises from the continuity and linear momentum balance equations for the solid species and the fluid through suitable constitutive assumptions and simplifications [18]. For equal-density particles, the velocities $v_1(\Phi), \ldots, v_N(\Phi)$ are given by

$$v_i(\Phi) = C(1 - \phi)V(\phi)\left(d_i^2 - \sum_{m=1}^{n} \phi_m d_m^2\right), \quad d_i := D_i/D_1, \quad i = 1, \ldots, N; \quad C = \frac{(\varrho_{\mathrm{s}} - \varrho_{\mathrm{f}})gD_1^2}{18\mu_{\mathrm{f}}}, \tag{2.6}$$

where $\phi := \phi_1 + \cdots + \phi_N$, ϱ_{s} and ϱ_{f} are the solid and fluid densities, g is the acceleration of gravity, μ_{f} is the fluid viscosity and V is an empirical hindrance function assumed to satisfy $V(0) = 1$, $V(\phi_{\max}) = 0$ and $V'(\phi) \leq 0$ for $\phi \in [0, \phi_{\max}]$. A standard choice for $V(\phi)$ is the Richardson-Zaki expression [19]:

$$V(\phi) = \begin{cases} (1 - \phi)^{n_{\mathrm{RZ}} - 2} & \text{for } 0 < \phi < \phi_{\max}, \\ 0 & \text{otherwise,} \end{cases} \quad n_{\mathrm{RZ}} > 2, \tag{2.7}$$

which we use in the following version with "soft cutoff" to avoid the discontinuity in the definition (2.7) for $\phi = \phi_{\max}$:

$$V(\phi) = \begin{cases} (1-\phi)^{n_{\mathrm{RZ}}-2} & \text{for } 0 < \phi < \phi_*, \\ V(\phi_*) + V'(\phi_*)(\phi - \phi_*) & \text{for } \phi_* \le \phi \le \phi_{\max}, \quad n_{\mathrm{RZ}} > 2. \\ 0 & \text{otherwise,} \end{cases} \tag{2.8}$$

where $\phi \mapsto \tau(\phi) := V(\phi_*) + V'(\phi_*)(\phi - \phi_*)$ is the tangent line to $V(\phi)$ at $(\phi_*, V(\phi_*))$, with ϕ_* being chosen such that $\tau(\phi_{\max}) = 0$. From this equation, and for $V(\phi)$ defined as in (2.7) we have

$$\phi_* = \frac{(n_{\mathrm{RZ}} - 2)\phi_{\max} - 1}{n_{\mathrm{RZ}} - 3}.$$

The MLB model (1.1), (1.2), (2.6) is strictly hyperbolic whenever $\phi_i > 0$ and $\phi < \phi_{\max}$ [3]. The eigenvalues $\lambda_i(\Phi)$ of $\mathcal{J}_{\boldsymbol{f}}(\Phi)$ satisfy the interlacing property (2.3) with the lower bound

$$M_1(\Phi) = C\left(d_N^2 V(\phi) + \big((1-\phi)V'(\phi) - 2V(\phi)\big) \sum_{m=1}^{N} d_m^2 \phi_m \right). \tag{2.9}$$

2.3. **Multiclass Lighthill-Whitham-Richards (MCLWR) traffic model.** The LWR kinematic traffic model describes the evolution of vehicle density $\phi(x,t)$ by a scalar conservation law $\partial_t \phi + \partial_x(\phi v(\phi)) = 0$, where the velocity function $v(\phi)$ is nonnegative and nonincreasing with respect to density ($v' \le 0$). In [10, 11] this model is generalized to multiple classes of drivers, with individual densities $\phi_i(x,t)$ ($i = 1, \dots, N$) evolving by LWR-like equations

$$\partial_t \phi_i + \partial_x f_i(\phi_1, \dots, \phi_N) = 0, \quad f_i(\phi_1, \dots, \phi_N) = \phi_i v_i(\phi), \tag{2.10}$$

coupled by $\phi = \phi_1 + \cdots + \phi_N$. The basic assumption of the MCLWR model is that

$$v_i(\phi) = \beta_i v(\phi), \quad i = 1, \dots, N, \tag{2.11}$$

i.e., drivers of different classes adjust their speed to the total traffic density ϕ through the same function $v(\phi)$, and β_i is the free-flowing speed of users in class i on an empty highway. The behavioral law $\phi \mapsto v(\phi)$ may be taken from standard speed-density relations like the Greenshields model $v(\phi) = 1 - \phi/\phi_{\max}$ [20], where $\phi_{\max}$ denotes a maximal car density, or the Drake model [21]

$$v(\phi) = \exp(-(\phi/\phi_{\mathrm{opt}})^2/2), \tag{2.12}$$

where the parameter ϕ_{opt} is an "optimal" density (that maximizes $\phi v(\phi)$). It is further assumed that $\beta_1 > \cdots > \beta_N > 0$.

It can be seen in [4,22] that the MCLWR model (1.1), (1.2), (2.11) is strictly hyperbolic whenever $\phi_i > 0$ and $\phi < \phi_{\max}$. The eigenvalues $\lambda_i = \lambda_i(\Phi)$ of the Jacobian $\mathcal{J}_{\boldsymbol{f}}(\Phi)$ satisfy the interlacing property (2.3), where the lower bound is given by

$$M_1(\Phi) = v_N(\phi) + v'(\phi) \sum_{i=1}^{N} \beta_i \phi_i. \tag{2.13}$$

It is common in traffic flow modeling to study the evolution of vehicular traffic on a circular road of length L, so for this application (1.1), (1.2) is studied along with the initial condition (2.4) and the periodic boundary condition

$$\Phi(0,t) = \Phi(L,t), \quad t > 0. \tag{2.14}$$

3. Polynomial viscosity matrix (PVM) schemes

3.1. **Roe matrices.** To focus on the main idea, let us concentrate for the moment on the discretization for the initial value problem of (1.1) for $x \in \mathbb{R}$. Assume that Δx and Δt are the spatial meshwidth and time step, respectively, of a standard Cartesian grid on $\mathbb{R} \times [0, \infty)$. We define $x_i = (i + 1/2)\Delta x$, $i \in \mathbb{Z}$, and $t_n = n\Delta t$, $n \in \mathbb{N}_0$. Then the finite volume formulation of (1.1) is

$$\frac{\mathrm{d}\bar{\Phi}_i(t)}{\mathrm{d}t} = -\frac{1}{\Delta x}\left(\boldsymbol{f}(\Phi(x_{i+1/2}, t)) - \boldsymbol{f}(\Phi(x_{i-1/2}, t))\right), \tag{3.1}$$

where we define

$$\bar{\Phi}_i(t) = \frac{1}{\Delta x}\int_{x_{i-1/2}}^{x_{i+1/2}} \Phi(\xi, t)\,\mathrm{d}\xi, \quad i \in \mathbb{Z}.$$

This leads to the following semi-discretization of (3.1) for $\Phi_i(t) \approx \bar{\Phi}_i(t)$:

$$\frac{\mathrm{d}\Phi_i(t)}{\mathrm{d}t} = -\frac{1}{\Delta x}\big(\hat{\boldsymbol{f}}_{i+1/2} - \hat{\boldsymbol{f}}_{i-1/2}\big), \quad i \in \mathbb{Z}, \tag{3.2}$$

where $\hat{\boldsymbol{f}}_{i+1/2}$ is a numerical flux that depends on values of Φ on a stencil around $x_{i+1/2}$. The ordinary differential equations (ODEs) (3.2) can be solved by a suitable ODE integrator (we use here Runge-Kutta methods), which gives the final fully discrete form

$$\Phi_i^{n+1} = \Phi_i^n - \frac{\Delta t}{\Delta x}\big(\tilde{\boldsymbol{f}}_{i+1/2}^n - \tilde{\boldsymbol{f}}_{i-1/2}^n\big), \quad i \in \mathbb{Z}, \quad n = 0, 1, 2, \ldots,$$

with numerical fluxes $\tilde{\boldsymbol{f}}_{i+1/2}^n$ obtained from $\hat{\boldsymbol{f}}_{i+1/2}$. For the first-order version, we use Euler's method:

$$\Phi_i^{n+1} = \Phi_i^n - \frac{\Delta t}{\Delta x}\big(\hat{\boldsymbol{f}}_{i+1/2}^n - \hat{\boldsymbol{f}}_{i-1/2}^n\big), \quad i \in \mathbb{Z}, \quad n = 0, 1, 2, \ldots,$$

where $\hat{\boldsymbol{f}}_{i+1/2}^n = \hat{\boldsymbol{f}}(\Phi_i^n, \Phi_{i+1}^n)$. One can obtain high order numerical methods from suitable reconstructions techniques (MUSCL, ENO, WENO), first-order methods such as Roe's method [1], and higher-order ODE integrators.

The numerical flux function for Roe's solver is based on a matrix $\boldsymbol{A} = \boldsymbol{A}(\Phi_\mathrm{L}, \Phi_\mathrm{R})$ that satisfies:

(1) Hyperbolicity of the system: $\boldsymbol{A}$ is diagonalizable with real eigenvalues.
(2) Consistency with the exact Jacobian: $\boldsymbol{A}(\Phi_\mathrm{L}, \Phi_\mathrm{R}) \to \mathcal{J}_{\boldsymbol{f}}(\Phi)$ smoothly as $\Phi_\mathrm{L}, \Phi_\mathrm{R} \to \Phi$.
(3) Conservation across discontinuities: $\boldsymbol{f}(\Phi_\mathrm{R}) - \boldsymbol{f}(\Phi_\mathrm{L}) = \boldsymbol{A}(\Phi_\mathrm{R} - \Phi_\mathrm{L})$.

The numerical flux function is then given by (1.3), where the matrix $|\boldsymbol{A}|$ is defined through the eigendecomposition $\boldsymbol{A} = \boldsymbol{R}\boldsymbol{\Lambda}\boldsymbol{R}^{-1}$, where $\boldsymbol{\Lambda} := \mathrm{diag}(\lambda_1, \ldots, \lambda_N)$ and $\lambda_1, \ldots, \lambda_N$ are the eigenvalues of $\boldsymbol{A}$, as follows:

$$|\boldsymbol{A}| := \boldsymbol{R}|\boldsymbol{\Lambda}|\boldsymbol{R}^{-1}, \quad |\boldsymbol{\Lambda}| = \mathrm{diag}\big(|\lambda_1|, \ldots, |\lambda_N|\big).$$

One way to guarantee that both conditions (1) and (2) are satisfied is to take

$$\boldsymbol{A} = \mathcal{J}_{\boldsymbol{f}}\left(\frac{1}{2}(\Phi_\mathrm{R} + \Phi_\mathrm{L})\right). \tag{3.3}$$

Unfortunately, this simple choice of $\boldsymbol{A}$ does not satisfy (3) in general. Roe matrices (that satisfy (1), (2) and (3)) can be obtained for some equations, such as Euler equations for gas dynamic, shallow waters equations, etc. For the general case, Harten et al. proved in [23] that a Roe matrix exists if the system is provided with an entropy. It is known that the MCLWR model (2.10) possesses an entropy [10], but it is not clear whether the MLB model does.

3.2. **Polynomial viscosity matrices.** PVM methods [5] constitute an alternative to obtain numerical methods for hyperbolic conservation laws when the computational cost for obtaining the eigenstructure of $\boldsymbol{A}$ is high. PVM methods replace $|\boldsymbol{A}(\Phi_{\mathrm{L}},\Phi_{\mathrm{R}})|$ in (1.3) by an approximation, based on some polynomial $P(x)=P(x;\Phi_{\mathrm{L}},\Phi_{\mathrm{R}})$,

$$\big|\boldsymbol{A}(\Phi_{\mathrm{L}},\Phi_{\mathrm{R}})\big| \approx P\big(\boldsymbol{A}(\Phi_{\mathrm{L}},\Phi_{\mathrm{R}})\big) \tag{3.4}$$

to define the numerical flux function:

$$\hat{\boldsymbol{f}}(\Phi_{\mathrm{L}},\Phi_{\mathrm{R}}) = \frac{1}{2}\big(\boldsymbol{f}(\Phi_{\mathrm{L}})+\boldsymbol{f}(\Phi_{\mathrm{R}})-P(\boldsymbol{A})(\Phi_{\mathrm{R}}-\Phi_{\mathrm{L}})\big). \tag{3.5}$$

Here it is understood that if $P(x)=\alpha_0+\alpha_1 x+\alpha_2 x^2+\cdots+\alpha_d x^d$ for $x\in\mathbb{R}$, where d is the degree of the polynomial and $\alpha_0,\dots,\alpha_d$ are real coefficients, then $P(\boldsymbol{A})=\alpha_0\boldsymbol{I}+\alpha_1\boldsymbol{A}+\alpha_2\boldsymbol{A}^2+\cdots+\alpha_d\boldsymbol{A}^d$ for any square matrix $\boldsymbol{A}$, where $\boldsymbol{I}$ denotes the identity matrix.

The goal in the design of the polyomial P is to use some knowledge on the eigenvalues of $\tilde{\boldsymbol{A}}$ to get (3.4) as accurate as possible. The key point is to achieve that $P(x)\approx|x|$ for x in some interval $\mathcal{I}$ containing all the eigenvalues of $\boldsymbol{A}$. If $\mathcal{I}$ is tight, then a better approximation is obtained. But, of course, $\mathcal{I}$ should be obtained without explicit knowledge of the eigenvalues. For instance, it is easy to see that (3.4) is exact if P interpolates all the eigenvalues of $\boldsymbol{A}$, but this would not be of practical use. It can be seen [6] that the scheme is L^∞-stable if

$$|x|\le P(x;\Phi_i,\Phi_{i+1}) \le \frac{\Delta x}{\Delta t} \quad \text{for all } x\in\mathcal{I},$$

where $\mathcal{I}$ is an interval containing the eigenvalues of $\boldsymbol{A}(\Phi_i,\Phi_{i+1})$.

3.3. **Some PVM methods.** The following PVM methods can be obtained from bounds on the eigenvalues $\lambda_1\ge\lambda_2\ge\cdots\ge\lambda_N$ of the Roe matrix (see [6]).

3.3.1. *Rusanov method.* This method is based on a bound $S_0\ge\max_j|\lambda_j|$, so that we can take $\mathcal{I}=[-S_0,S_0]$ and the zero-degree polynomial that interpolates $|x|$ at S_0 is simply $P_0(x)=S_0$. The corresponding numerical flux obtained from setting $P(\boldsymbol{A})=S_0\boldsymbol{I}$ in (3.5) is that of the well-known Rusanov method.

3.3.2. *HLL method.* Assume that we bounds $S_{\mathrm{L}}\le\lambda_j\le S_{\mathrm{R}}$, $j=1,\dots,N$, are available, so that we can take $\mathcal{I}=[S_{\mathrm{L}},S_{\mathrm{R}}]$ and define $P_1(x)=\alpha_0+\alpha_1 x$ to be the first-degree polynomial that interpolates $|x|$ at $S_{\mathrm{L}},S_{\mathrm{R}}$. This yields the numerical flux of the known Harten, Lax and van Leer (HLL) method [23], namely

$$\hat{\boldsymbol{f}}^{\mathrm{HLL}}_{i+1/2} = \frac{1}{S_{\mathrm{R}}-S_{\mathrm{L}}}\big(S_{\mathrm{R}}\boldsymbol{f}(\Phi_i)-S_{\mathrm{L}}\boldsymbol{f}(\Phi_{i+1})+S_{\mathrm{R}}S_{\mathrm{L}}(\Phi_{i+1}-\Phi_i)\big).$$

This flux can be modified when S_{L} and S_{R} have the same sign to give the upwind numerical flux, such that

$$\hat{\boldsymbol{f}}_{i+1/2} = \begin{cases} \boldsymbol{f}(\Phi_i) & \text{if } S_{\mathrm{L}}\ge 0,\\ \hat{\boldsymbol{f}}^{\mathrm{HLL}}_{i+1/2} & \text{if } S_{\mathrm{L}}\le 0\le S_{\mathrm{R}},\\ \boldsymbol{f}(\Phi_{i+1}) & \text{if } S_{\mathrm{R}}\le 0. \end{cases}$$

3.3.3. *PVM-2(S_0) method or FORCE-type methods.* This method is based on a bound $S_0\ge\max_j|\lambda_j|$ and takes a second-degree polynomial $P_2(x)=\alpha_0+\alpha_2x^2$ such that $P_2(S_0)=S_0$ and $P_2'(S_0)=1$ to obtain the numerical flux.

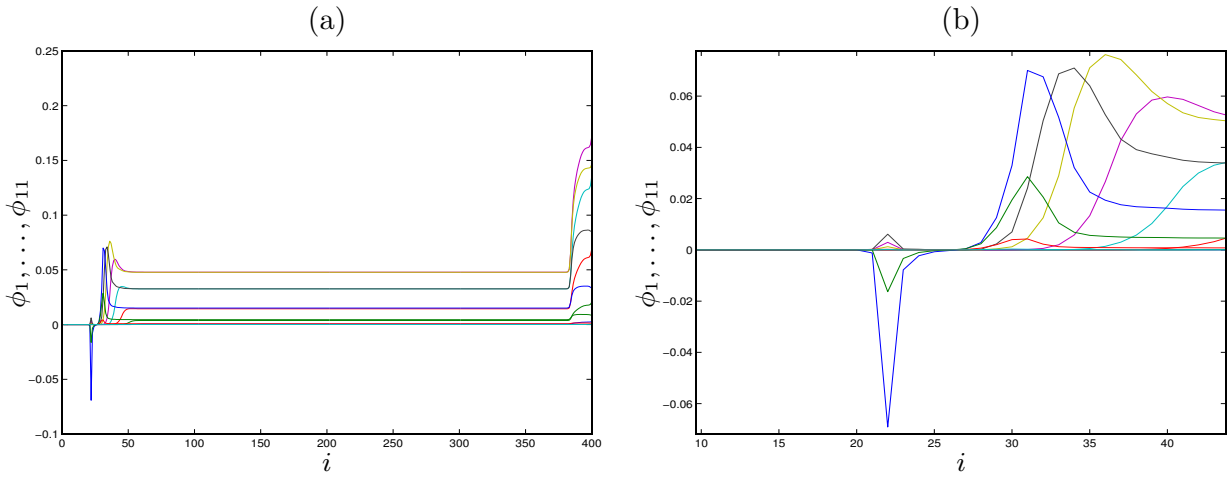

FIGURE 1. Oscillatory numerical solution produced by method PVM-4(S_M, S_I) with $N = 11$ species and cfl $= 0.5$. The comuputational domain is subdivided into $M = 400$ cells. (a) Snapshot of the numerical solution, (b) enlarged view.

3.3.4. *PVM-2*(S_M, S_m) *method.* This method is based on bounds $S_{\mathrm{L}} \le \lambda_j \le S_{\mathrm{R}}$, $j = 1, \ldots, N$ and considers a second-degree polynomial $P_2(x) = \alpha_0 + \alpha_1 x + \alpha_2 x^2$ such that

$$P_2(S_m) = |S_m|, \quad P_2(S_M) = |S_M|, \quad P_2'(S_M) = \mathrm{sgn}(S_M)$$

where S_m, respectively, S_M are the elements with the minimum, respectively, maximum absolute value of $\{S_{\mathrm{L}}, S_{\mathrm{R}}\}$.

3.3.5. *PVM-4*(S_M, S_I) *and PVM-4*(S_0) *methods.* These methods are based on utilizing

$$P_4(x) = \alpha_0 + \alpha_2 x^2 + \alpha_4 x^4, \quad \text{such that } P_4(S_M) = |S_M|,\ P_4(S_I) = S_I \text{ and } P_4'(S_I) = 1, \tag{3.6}$$

where S_M and S_I are the first and second elements of the list of eigenvalue ordered by decreasing absolute value. Then one can compute

$$\alpha_0 = \frac{|S_M||S_I|(|S_I| + 2|S_M|)}{2(|S_I| + |S_M|)^2}, \quad \alpha_2 = \frac{1}{2|S_M|} + \frac{|S_M|}{(|S_I| + |S_M|)^2}, \quad \alpha_4 = -\frac{1}{2|S_M|(|S_I| + |S_M|)^2}. \tag{3.7}$$

If $S_M = S_I = S_0$ then these coefficients reduce to

$$\alpha_0 = \frac{3S_0}{8}, \quad \alpha_2 = \frac{3}{4S_0}, \quad \alpha_4 = -\frac{1}{8S_0^3}.$$

This method will be denoted as PVM-4(S_0).

As we see in Figure 1, corresponding to a preliminary numerical experiment with $N = 11$ species (cf. Example 3 to be presented in Section 4.2), strong oscillations are generated in the region corresponding to clear liquid. These oscillations disappeared reducing the Courant number $|S_M|\Delta t/\Delta x$ to 0.01. This fact alerted us to a possible violation of the constraint

$$\frac{\|P_l\|_\infty \Delta t}{\Delta x} \le 1, \tag{3.8}$$

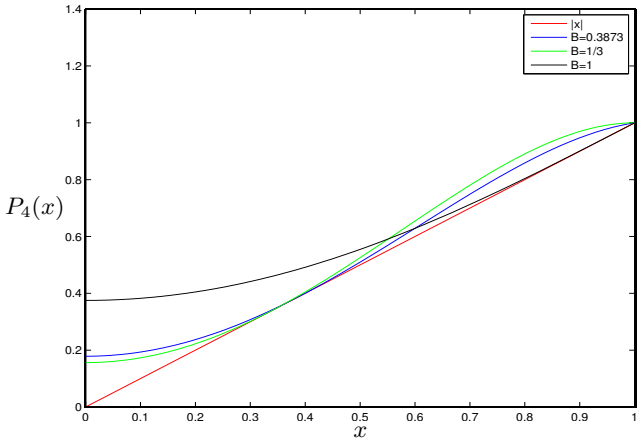

FIGURE 2. Comparison of P_4, defined by (3.6), (3.7), for $|S_M| = A = 1$ and different choices of $S_I = B$.

which is indeed the case, as we next detail. For notational simplicity, we write A, B instead of $|S_M|, S_I$, respectively. It can be proven that P_4 has a unique local maximum in $(0, \infty)$, given by

$$c = -\frac{\alpha_2}{2\alpha_4} = 2B^2 + (A+B)^2 \quad \text{and} \quad P_4(c) = B + \frac{(A+B)^2}{8B}.$$

If it happens that $B \ll A$ and $c \in (0, A)$, then it turns out that $P_4(c) \gg A = |S_M|$ and the restriction in (3.8) is much more severe than

$$\frac{|S_M|\Delta t}{\Delta x} \leq 1.$$

Since $B \in (0, A)$ is arbitrary we propose to set it such that

$$\max_{x\in[0,A]} P_4(x) = \max_{x\in[-A,A]} P_4(x) = P_4(A) = A,$$

which yields $B = A/3$.

We propose another option, which is considering $B \in [0, A]$ that minimizes

$$\Phi_A(B) = \int_0^A (P_4[A, B](x) - x)^2 \, \mathrm{d}x.$$

Since $\lim_{B\to 0} \Phi_A(B) = \infty$, the minimum is attained either at $B = A$ or at $B \in (0, A)$ such that $\Phi_A'(B) = 0$, which can be written as:

$$0 = -16 + 33\frac{B}{A} + 66\left(\frac{B}{A}\right)^2 - 210\left(\frac{B}{A}\right)^3 + 42\left(\frac{B}{A}\right)^4 + 525\left(\frac{B}{A}\right)^5 =: q\left(\frac{B}{A}\right).$$

The only positive root of q is ≈ 0.3873. The polynomials obtained with $A = 1$, $B = 0.3873, 1/3, 1$ appear in Figure 2.

3.4. **PVM methods for kinematic flow models.** There are specific issues about the implementation of PVM methods for kinematic flow models. The first one is the general unavailability of Roe matrices and the second one is bounding eigenvalues. For the first issue, we propose to use

approximate Roe matrices, i.e., matrices that satisfy the defining properties approximately. For this purpose, we consider the equation

$$\boldsymbol{f}(\Phi_{\mathrm{R}}) - \boldsymbol{f}(\Phi_{\mathrm{L}}) = \bar{\boldsymbol{A}}(\Phi_{\mathrm{L}}, \Phi_{\mathrm{R}})(\Phi_{\mathrm{R}} - \Phi_{\mathrm{L}}), \quad \bar{\boldsymbol{A}} = \int_0^1 \mathcal{J}_{\boldsymbol{f}}\big(\Phi_{\mathrm{L}} + s(\Phi_{\mathrm{R}} - \Phi_{\mathrm{L}})\big)\,\mathrm{d}s. \tag{3.9}$$

This definition satisfies the second and third properties of Roe matrices, but the real diagonalizability of $\mathcal{J}_{\boldsymbol{f}}(\Phi_{\mathrm{L}} + s(\Phi_{\mathrm{R}} - \Phi_{\mathrm{L}}))$ does not need to carry over to $\bar{\boldsymbol{A}}$. Specifically, we will use matrices $\boldsymbol{A}$ that approximate $\bar{\boldsymbol{A}}$ by using the midpoint rule (3.3), a two-node Gaussian formula

$$\boldsymbol{A} = \frac{1}{2}\mathcal{J}_{\boldsymbol{f}}\left(\Phi_{\mathrm{L}} + \frac{1 - 1/\sqrt{3}}{2}(\Phi_{\mathrm{R}} - \Phi_{\mathrm{L}})\right) + \frac{1}{2}\mathcal{J}_{\boldsymbol{f}}\left(\Phi_{\mathrm{L}} + \frac{1 + 1/\sqrt{3}}{2}(\Phi_{\mathrm{R}} - \Phi_{\mathrm{L}})\right) \tag{3.10}$$

or a three-node Gaussian formula

$$\begin{aligned}\boldsymbol{A} = {} & \frac{5}{18}\mathcal{J}_{\boldsymbol{f}}\left(\Phi_{\mathrm{L}} + \frac{1 - \sqrt{3}/\sqrt{5}}{2}(\Phi_{\mathrm{R}} - \Phi_{\mathrm{L}})\right) + \frac{4}{9}\mathcal{J}_{\boldsymbol{f}}\left(\frac{\Phi_{\mathrm{L}} + \Phi_{\mathrm{R}}}{2}\right) \\ & + \frac{5}{18}\mathcal{J}_{\boldsymbol{f}}\left(\Phi_{\mathrm{L}} + \frac{1 + \sqrt{3}/\sqrt{5}}{2}(\Phi_{\mathrm{R}} - \Phi_{\mathrm{L}})\right)\end{aligned} \tag{3.11}$$

(at the risk of not being real diagonalizable, an issue that we have not experienced in our numerical tests).

For the second issue, in Section 3.3 we have not fully specified which eigenvalues are dealt with in the formulae defining each method. In any case, we can use $M_1(\Phi)$ in (2.9) or (2.13) and $M_2 = v_1(\Phi)$ to obtain the required bounds, as long as the referring matrix is a Jacobian of fluxes. But there is another point here that should be taken into account: the fluxes are not genuinely nonlinear, which in the scalar case corresponds to the flux having inflection points, and the interval where the eigenvalues lie should be considered more carefully. Our proposal is to consider not only the matrices $\boldsymbol{A}$, $\mathcal{J}_{\boldsymbol{f}}(\Phi_{\mathrm{L}})$ and/or $\mathcal{J}_{\boldsymbol{f}}(\Phi_{\mathrm{R}})$ but all the matrices $\mathcal{J}_{\boldsymbol{f}}(\Phi_{\mathrm{L}} + s(\Phi_{\mathrm{R}} - \Phi_{\mathrm{L}}))$, $s \in [0, 1]$ to compute, for instance, $\min_{0\le s\le 1} M_1(\Phi_{\mathrm{L}} + s(\Phi_{\mathrm{R}} - \Phi_{\mathrm{L}}))$ or $\max_{0\le s\le 1} M_2(\Phi_{\mathrm{L}} + s(\Phi_{\mathrm{R}} - \Phi_{\mathrm{L}}))$ as lower, respectively, upper bound for the eigenvalues.

3.5. **MUSCL extrapolation.** We use the MUSCL technique (see [24]) to obtain second-order schemes from the basic first-order PVM schemes. Following this technique, one defines the numerical flux as follows, where $\boldsymbol{\Phi} = \{\Phi_i\}_{i\in\mathbb{Z}}$:

$$\hat{\boldsymbol{f}}_{i+1/2} = \hat{\boldsymbol{f}}_{i+1/2}(\boldsymbol{\Phi}) = \hat{\boldsymbol{f}}(\Phi_{i-1}, \Phi_i, \Phi_{i+1}, \Phi_{i+2}) = \hat{\boldsymbol{f}}^{\mathrm{PVM}}\big(\Phi^-_{i+1/2}, \Phi^+_{i+1/2}\big),$$

where $\hat{\boldsymbol{f}}^{\mathrm{PVM}}$ denotes one of the first-order PVM fluxes defined so far and the extrapolated solution vectors $\Phi^{\pm}_{i\mp1/2}$ are defined by

$$\Phi^{\pm}_{i\mp1/2} = \Phi_i \mp \frac{1}{2}\,\mathrm{minmod}(\Phi_i - \Phi_{i-1}, \Phi_{i+1} - \Phi_i),$$

where the standard minmod function is defined by

$$\mathrm{minmod}(a, b) = \frac{1}{2}\big(\mathrm{sgn}(a) + \mathrm{sgn}(b)\big)\min\big\{|a|, |b|\big\}.$$

We use Heun's method to obtain the following final fully discrete scheme, where $\boldsymbol{\Phi}^n = \{\Phi^n_i\}_{i\in\mathbb{Z}}$ and $\boldsymbol{\Phi}^{(k)} = \{\Phi^{(k)}_i\}_{i\in\mathbb{Z}}$ for $k = 1, 2$:

$$\Phi^{(1)}_i = \Phi^n_i - \frac{\Delta t}{\Delta x}\big(\hat{\boldsymbol{f}}_{i+1/2}(\boldsymbol{\Phi}^n) - \hat{\boldsymbol{f}}_{i-1/2}(\boldsymbol{\Phi}^n)\big),$$

$$\Phi_i^{(2)} = \Phi_i^{(1)} - \frac{\Delta t}{\Delta x}\big(\hat{\boldsymbol{f}}_{i+1/2}(\boldsymbol{\Phi}^{(1)}) - \hat{\boldsymbol{f}}_{i-1/2}(\boldsymbol{\Phi}^{(1)})\big),$$
$$\Phi_i^{n+1} = \frac{1}{2}\big(\Phi_i^n + \Phi_i^{(2)}\big), \quad i \in \mathbb{Z}, \quad n = 0, 1, 2, \ldots.$$

To complete the description, we mention that the boundary conditions are discretized by setting

$$\Phi_i^n = \mathbf{0} \quad \text{for } i = -1, -2, \quad \Phi_{M+i+1}^n = (\phi_{\max}, \ldots, \phi_{\max})^{\mathrm{T}} \quad \text{for } i = 1, 2 \tag{3.12}$$

for (2.5) and by

$$\Phi_i^n = \Phi_{M+i}^n, \quad \Phi_{M+2+i}^n = \Phi_{2+i}^n \quad \text{for } i = 1, 2$$

in the case of (2.14). We recall that a MUSCL scheme requires to consider two additional ghost cells on each boundary of the computational domain. The second condition of (3.12) ensures that the total concentration at the bottom is the maximum.

4. Numerical results

4.1. **Preliminaries.** In the following examples, we solve (1.1) numerically for $0 \le t \le T$ and $0 \le x \le L$ for the MLB polydisperse sedimentation model and the MCLWR traffic model. We compare numerical results obtained by some chosen PVM methods with a high-order characteristic-wise numerical method (SPEC-INT), based on fifth-order finite difference weighted essentially non-oscillatory (WENO) schemes, see [13] for the details.

For each model, the x-interval $[0, L]$ is subdivided into M subintervals of length $\Delta x = L/M$. We denote by Δt the time step used to advance the numerical solution from $t = t^n$ to $t^{n+1} = t^n + \Delta t$ and by Φ_j^n the vector of numerical solutions associated with cell $[j\Delta x, (j+1)\Delta x]$, $j = 0, \ldots, M-1$, at time t^n. For each iteration, Δt is determined by the following formula (CFL condition):

$$\frac{\Delta t}{\Delta x} \max_{1 \le j \le M} \varrho\big(\mathcal{J}_{\boldsymbol{f}}(\Phi_j^n)\big) = C_{\mathrm{cfl}},$$

where $\varrho(\cdot)$ is the spectral radius (or an upper bound of it). In the numerical examples we choose $C_{\mathrm{cfl}} = 0.6$.

For comparison purposes, we compute reference solutions for numerical tests by the SPEC-INT scheme with $M_{\mathrm{ref}} = 12800$ cells. We compute approximate L^1 errors at different times for each scheme as follows. We denote by $(\phi_{j,i}^M(t))_{j=1}^M$ and $(\phi_{l,i}^{\mathrm{ref}}(t))_{l=1}^{M_{\mathrm{ref}}}$ the numerical solution for the i-th component at time t calculated with M and M_{ref} cells, respectively. We compute $\tilde{\phi}_{j,i}^{\mathrm{ref}}(t)$ for $j = 1, \ldots, M$ by

$$\tilde{\phi}_{j,i}^{\mathrm{ref}}(t) = \frac{1}{R}\sum_{k=1}^{R} \phi_{R(j-1)+k,i}^{\mathrm{ref}}(t), \quad R = M_{\mathrm{ref}}/M.$$

The total approximate L^1 error of the numerical solution $(\phi_{j,i}^M(t))_{j=1}^M$ at time t is then given by

$$e_M^{\mathrm{tot}}(t) := \frac{1}{M}\sum_{i=1}^{N}\sum_{j=1}^{M} \big|\tilde{\phi}_{j,i}^{\mathrm{ref}}(t) - \phi_{j,i}^M(t)\big|. \tag{4.1}$$

Based on the approximate errors defined by (4.1), we may calculate a numerical order of convergence from pairs of total approximate L^1 errors $e_{M/2}^{\mathrm{tot}}(t)$ and $e_M^{\mathrm{tot}}(t)$ by

$$\theta_M(t) := \log_2\big(e_{M/2}^{\mathrm{tot}}(t)/e_M^{\mathrm{tot}}(t)\big).$$

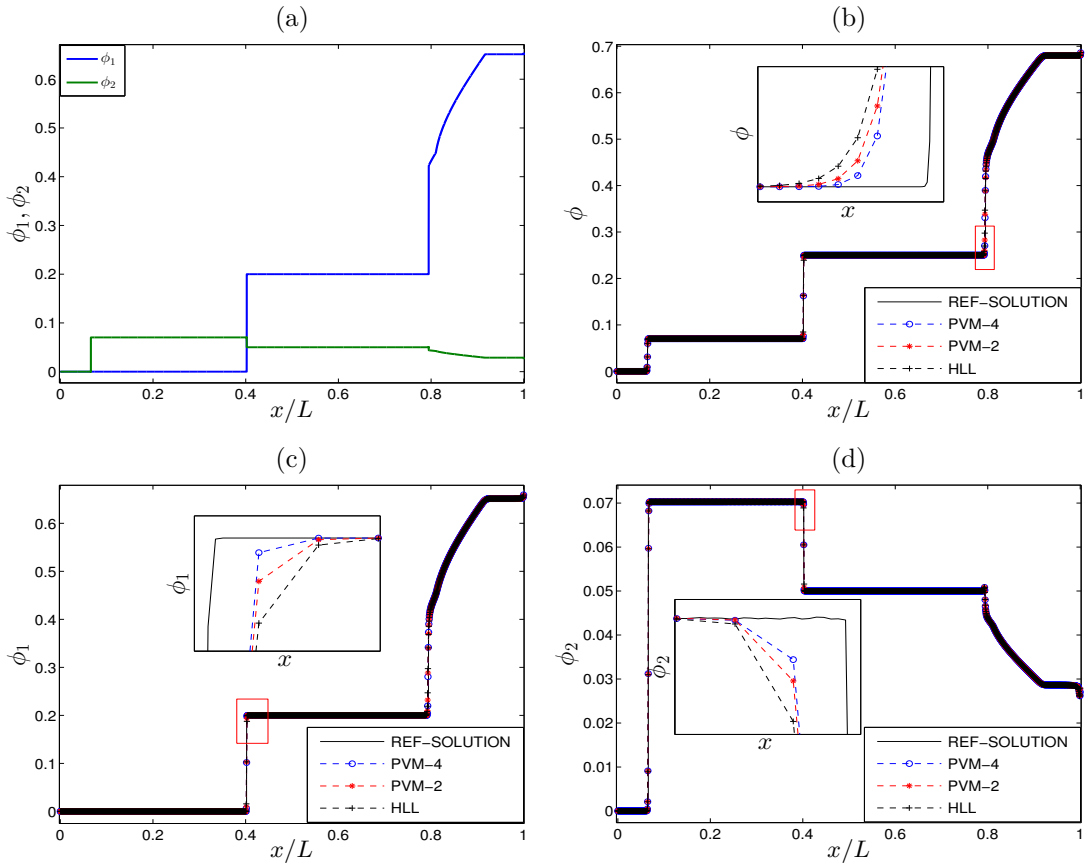

FIGURE 3. Example 1 (MLB model, $N = 2$): numerical solution for ϕ, ϕ_1, ϕ_2 at $T = 50\,\mathrm{s}$ computed (a) by SPEC-INT method with $M = M_{\mathrm{ref}}$=12800 (reference solution), (b, c, d) by PVM methods with $M = 1600$, including the reference solution.

4.2. **Examples 1, 2 and 3 (MLB model, $N = 2, 4, 11$).** In Examples 1 to 3 we consider the standard test case of batch settling of an initially homogeneous suspension in a column. Example 1 corresponds to $N = 2$ species [25] with density $\varrho_{\mathrm{s}} = 2790\,\mathrm{kg/m^3}$ and different diameters $D_1 = 4.96 \times 10^{-4}\,\mathrm{m}$ and $D_2 = 1.25 \times 10^{-4}\,\mathrm{m}$, corresponding to $d_1 = 1$ and $d_2 = D_2/D_1 = 0.25202$. The depth of the vessel is $L = 0.3\,\mathrm{m}$. The maximum total concentration is $\phi_{\max} = 0.6$ and the initial concentrations are $\Phi_0 = (\phi_1^0, \phi_2^0) = (0.2, 0.05)^{\mathrm{T}}$. The hindered settling factor $V(\phi)$ is chosen according to (2.8) with the exponent $n_{\mathrm{RZ}} = 4.7$. The remaining parameters are $g = 9.81\,\mathrm{m/s^2}$, $\mu_{\mathrm{f}} = 0.02416\,\mathrm{Pa\ s}$ and $\varrho_{\mathrm{f}} = 1208\,\mathrm{kg/m^3}$. To compare the performance of PVM methods with that of SPEC-INT, we calculate numerical solutions for a sequence of spatial discretizations $\Delta x = L/M$, and compare the solutions with the above-mentioned reference solution. The variant of the PVM-4 method employed for simulations is the one that corresponds to the choice $|S_M| = A = 1$ and $S_I = B = 0.3873$ (see Section 3.3.5). These solutions are shown in Figure 3 for the simulated time $T = 50\,\mathrm{s}$. We use the midpoint rule (3.3) to calculate the approximate Roe matrix $\boldsymbol{A}$. The approximate errors, convergence rates and CPU time for Examples 1 to 4 are shown in Table 2.

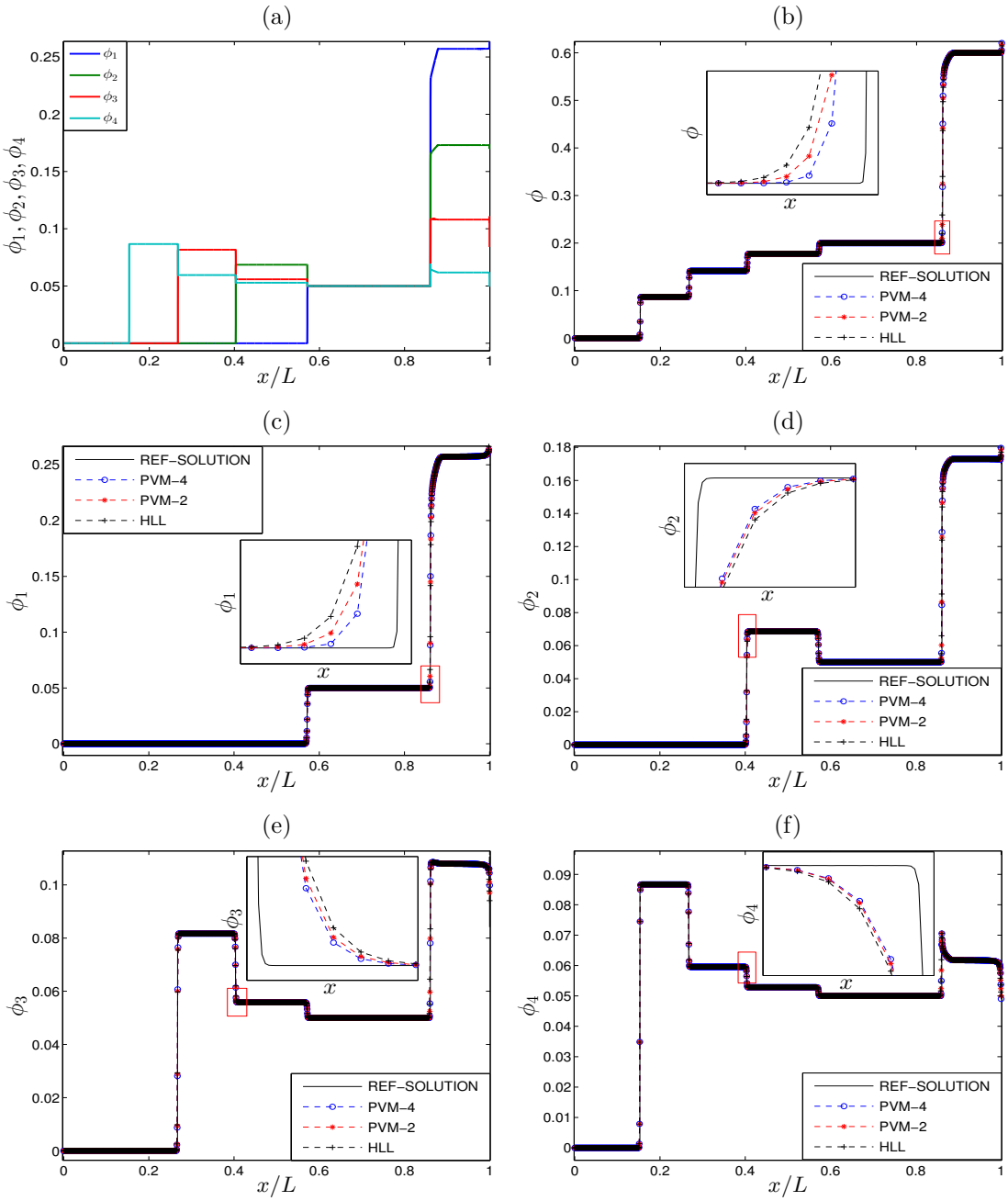

FIGURE 4. Example 2 (MLB model, $N = 4$): numerical solution for $\phi, \phi_1, \phi_2, \phi_3, \phi_4$ at $T = 50\,\mathrm{s}$ computed (a) by SPEC-INT with M_{ref}=12800 (reference solution), (b, c, d, e, f) by PVM methods with $M = 1600$, including the reference solution.

In Example 2 we consider the MLB model for $N = 4$ with paramters $d_1 = 1$, $d_2 = 0.8$, $d_3 = 0.6$, $d_4 = 0.4$, $\phi_{\max} = 0.6$, and $\phi_i^0 = 0.05$ for $i = 1, \ldots, 4$ The other parameters are the same as in Example 1. Numerical results at $T = 50\,\mathrm{s}$ are shown in Figure 4.

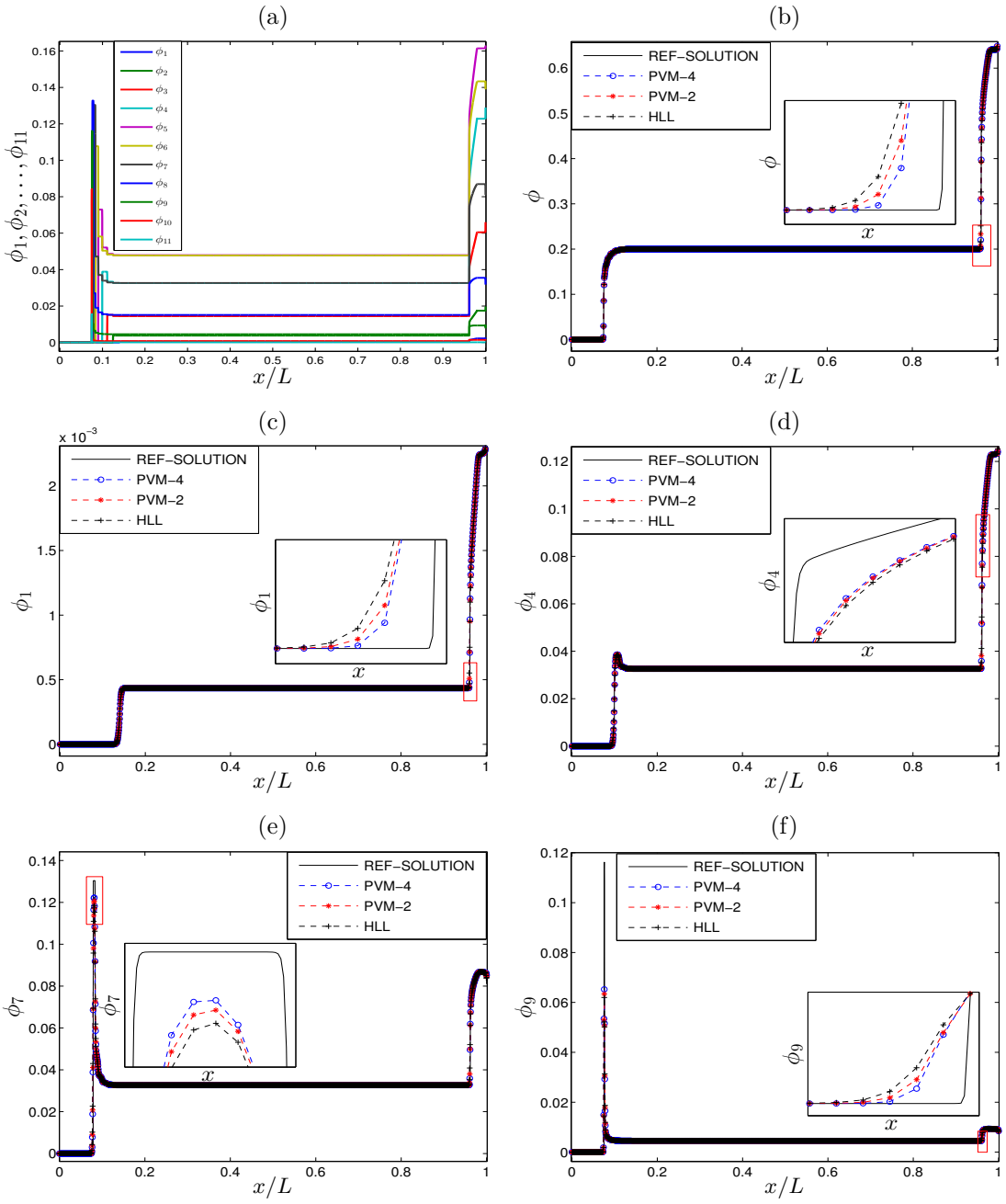

FIGURE 5. Example 3 (MLB model, $N = 11$): numerical solution for $\phi, \phi_1, \ldots, \phi_{11}$ at $T = 50\,\mathrm{s}$ (a) computed by (a) SPEC-INT with M_{ref}=12800 (reference solution), (b, c, d, e, f) by PVM methods with $M = 1600$, including the reference solution.

In Example 3 we simulate the MLB model for $N = 11$ species settling in a column of depth $L = 0.935\,\mathrm{m}$, according to an experiment published in [26]. The initial concentrations ϕ_i^0, diameters D_i and normalized $d_i = D_i/D_1$ are given in Table 1; we use again (2.8) with $n_{\mathrm{RZ}} = 4.7$ and the maximum total concentration $\phi_{\max} = 0.641$. Numerical results are shown in Figure 5.

i	1	2	3	4	5	6	7	8	9	10	11
$\phi_i^0[10^{-3}]$	0.435	3.747	14.420	32.603	47.912	47.762	32.663	15.104	4.511	0.783	0.060
$D_i[10^{-5}\text{m}]$	8.769	8.345	7.921	7.497	7.073	6.649	6.225	5.801	5.377	4.953	4.529
d_i	1.000	0.952	0.903	0.855	0.807	0.758	0.710	0.662	0.613	0.565	0.516

TABLE 1. Example 3 (MLB model, $N = 11$): initial concentrations ϕ_i^0 and real and normalized particle sizes D_i and d_i [26].

		SPEC-INT			HLL			PVM-2			PVM-4		
	M	e_M^{tot}	θ_M	cpu [s]	e_M^{tot}	θ_M	cpu [s]	e_M^{tot}	θ_M	cpu [s]	e_M^{tot}	θ_M	cpu [s]
Example 1	100	2.588	—	2.03	6.142	—	0.05	5.428	—	0.07	4.890	—	0.07
MLB model	200	1.620	0.676	3.75	3.760	0.708	0.21	3.352	0.695	0.28	3.068	0.673	0.29
$N = 2$	400	0.894	0.858	10.43	2.197	0.775	1.41	1.949	0.783	1.83	1.768	0.795	1.91
$T = 50\,\text{s}$	800	0.449	0.994	38.04	1.180	0.896	6.20	1.050	0.892	8.30	0.961	0.879	8.52
	1600	0.199	1.171	101.00	0.612	0.947	23.89	0.546	0.943	32.37	0.507	0.922	33.13
Example 2	100	5.104	—	5.97	10.436	—	0.07	9.404	—	0.10	8.683	—	0.1
MLB model	200	2.418	1.078	17.38	5.508	0.922	0.62	4.935	0.930	0.85	4.575	0.924	0.82
$N = 4$	400	1.275	0.924	43.40	3.017	0.869	2.21	2.716	0.861	3.06	2.554	0.841	3.15
$T = 50\,\text{s}$	800	0.708	0.848	75.44	1.678	0.846	7.17	1.524	0.834	9.97	1.451	0.816	10.18
	1600	0.312	1.185	221.18	0.825	1.024	26.78	0.750	1.023	37.34	0.719	1.012	39.04
Example 3	100	4.647	—	1.12	6.446	—	0.01	5.804	—	0.02	5.267	—	0.02
MLB model	200	2.980	0.641	5.16	4.525	0.510	0.06	4.139	0.488	0.09	3.880	0.441	0.10
$N = 11$	400	1.817	0.713	32.79	3.364	0.428	0.30	3.079	0.427	0.46	2.901	0.419	0.49
$T = 50\,\text{s}$	800	1.148	0.662	118.66	2.348	0.519	1.22	2.154	0.516	1.79	2.049	0.502	1.98
	1600	0.576	0.997	444.04	1.428	0.717	4.63	1.303	0.725	6.79	1.242	0.723	7.47
Example 4	100	1.690	—	0.26	3.467	—	0.02	3.461	—	0.02	3.495	—	0.02
MCLWR model	200	1.632	0.051	1.27	2.776	0.321	0.06	2.760	0.327	0.09	2.777	0.332	0.11
$N = 9$	400	1.130	0.530	4.16	1.932	0.523	0.27	1.900	0.538	0.39	1.883	0.561	0.43
$T = 0.015\,\text{h}$	800	0.794	0.509	19.89	1.408	0.457	1.13	1.384	0.458	1.63	1.358	0.471	1.81
	1600	0.441	0.849	63.11	0.913	0.625	5.07	0.895	0.628	7.29	0.870	0.642	7.94

TABLE 2. Examples 1 to 4: approximate L^1 errors (e_M^{tot}, figures to be multiplied by 10^{-3}), convergence rates (θ_M) and CPU times (cpu). The Roe matrix was approximated by the midpoint rule (3.3).

4.3. **Example 4 (MCLWR model, $N = 9$).** We consider the numerical experiment proposed in [27] where the initial density distribution is given by an isolated platoon in the congested regime for the Drake model (2.12) with $\phi_{\text{opt}} = 50\,\text{cars/km}$. We consider a nine-class system with $(\beta_1, \dots, \beta_9) = (60.0, 67.5, 75.0, \dots, 120.0)$ km/h and the initial datum

$$\Phi(x, 0) = p(x)\phi_0(0.04, 0.08, 0.12, 0.16, 0.2, 0.16, 0.12, 0.08, 0.04)^{\text{T}},$$

corresponding to a "platoon" defined by $\phi = \phi_0 = 120\,\text{cars/km}$ (which is well over the optimal density ϕ_{opt} and leads to a congested traffic regime) and the shape function

$$p(x) = \begin{cases} 10x & \text{for } 0 < x < 0.1, \quad 1 \quad \text{for } 0.1 < x \le 0.9, \\ -10(x-1) & \text{for } 0.9 < x \le 1, \quad 0 \qquad \text{otherwise.} \end{cases}$$

Numerical results are shown in Figure 6. Table 3 shows results corresponding to different forms of Gaussian quadrature applied to the integral in (3.9) to calculate the approximate Roe matrix.

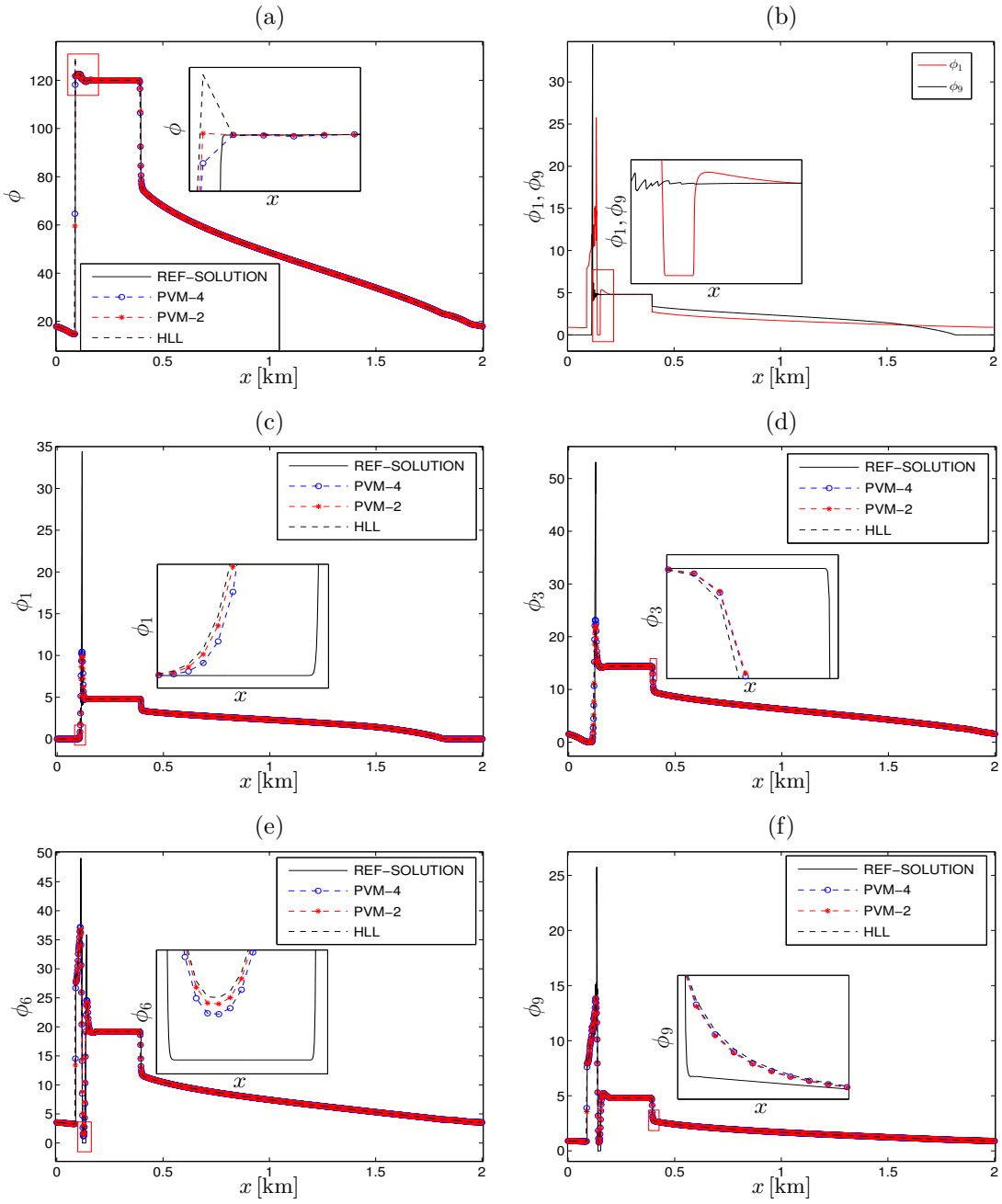

FIGURE 6. Example 4 (MCLWR model, $N = 9$): numerical solution (a) for ϕ and (b, c, d, e, f) for selected classes at $T = 0.015\,\mathrm{h}$ computed by SPEC-INT with M_{ref}=12800 (reference solution), and by PVM methods with $M = 1600$, including the reference solution.

No substancial difference is found in the approximate errors, whereas the CPU time required for the midpoint rule (3.3) is much smaller than for the Gaussian quadrature rules (3.10) and (3.11). This

		Gaussian quadrature, 2 nodes						Gaussian quadrature, 3 nodes					
		PVM-2			PVM-4			PVM-2			PVM-4		
	M	e_M^{tot}	θ_M	cpu [s]	e_M^{tot}	θ_M	cpu [s]	e_M^{tot}	θ_M	cpu [s]	e_M^{tot}	θ_M	cpu [s]
Example 3	100	5.804	—	0.03	5.267	—	0.04	5.804	—	0.05	5.267	—	0.06
MLB model	200	4.139	0.488	0.15	3.880	0.441	0.18	4.139	0.488	0.25	3.880	0.441	0.28
$N = 11$	400	3.079	0.427	0.74	2.901	0.419	0.83	3.079	0.427	1.20	2.901	0.419	1.29
$T = 50\,\text{s}$	800	2.154	0.516	2.93	2.049	0.502	3.34	2.154	0.516	4.68	2.049	0.502	5.17
	1600	1.303	0.725	11.29	1.242	0.723	12.79	1.303	0.725	17.91	1.242	0.723	19.85

TABLE 3. Example 3: approximate L^1 errors (e_M^{tot}, figures to be multiplied by 10^{-3}), convergence rates (θ_M) and CPU times (cpu) for approximation of the Roe matrix by Gaussian quadrature with two nodes (3.10) or three nodes (3.11).

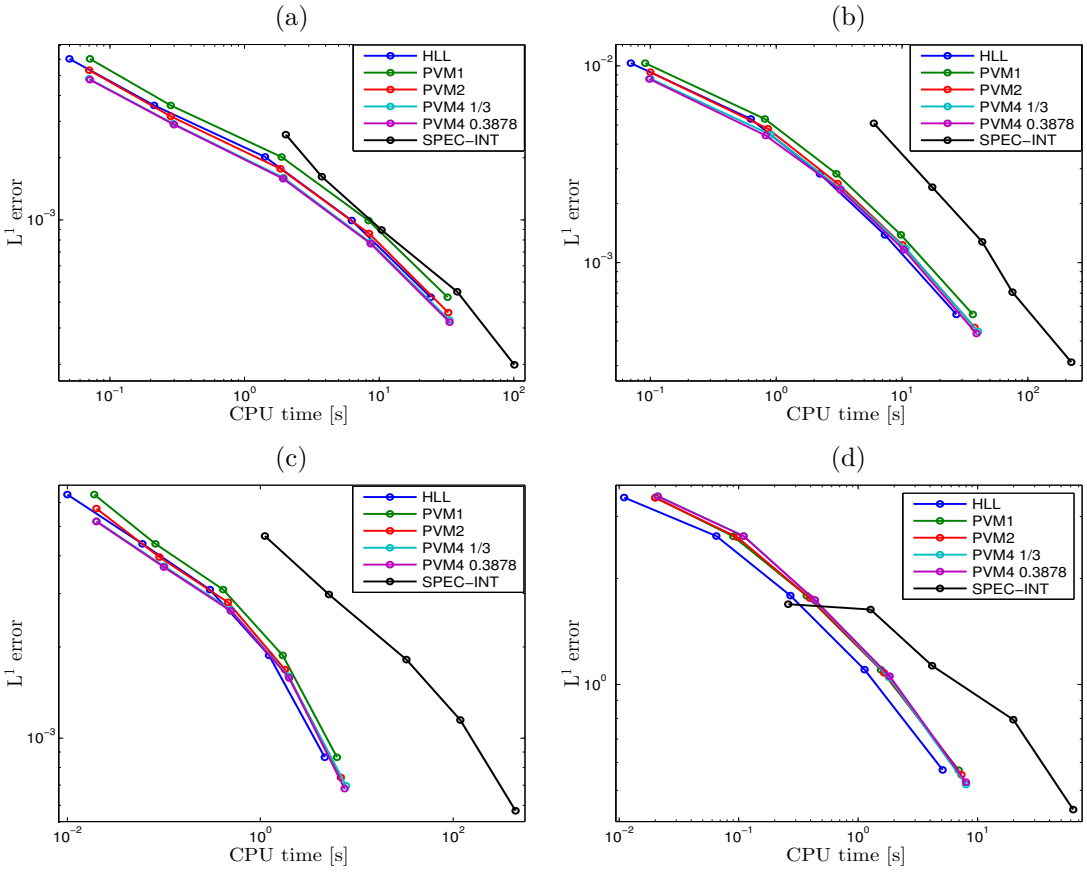

FIGURE 7. Examples 1 to 4: (MLB models $N = 2, 4, 11$, MCLWR model $N = 9$): Efficiency plot based on numerical solutions for $\Delta x = 1/M$ with $M = 100$, 200, 400, 800 and 1600: (a) Example 1, (b) Example 2, (c) Example 3, (d) Example 4.

is due to the fact that multiplication by a single Jacobian can be performed fastly by exploiting its structure.

4.4. **Efficiency plots.** Based on the information of Table 2 and considering several variants of the PVM-4 method we plot in Figure 7 approximate L^1 errors versus CPU time to assess which of the

methods examined is most efficient (in the usual sense of error reduction versus CPU time). It turns out that the methods PVM methods are roughly comparable in efficiency, and in turns out that in some cases and for coarse discretizations (e.g., for Example 3, as seen in Figure 7 (c)), the PVM-4 methods are most efficient. Moreover, for large values of N and fine discretizations, PVM methods are significantly more efficient than SPEC-INT.

5. Conclusions

In this paper we have proposed a fast numerical method that uses polynomial viscosity matrices to approximate Roe's numerical flux for polydisperse sedimentation simulations. We conclude that the best approximation is obtained by means of four degree polynomials (PVM-4) and an approximate Roe matrix given by the Jacobian of the fluxes computed at an average state. We have proposed two new PVM-4 schemes that improve the performance of the PVM-4 schemes proposed in [6], specially when the second largest eigenvalue is very close to zero with respect to the largest eigenvalue.

Another contribution of this work is the efficiency test of PVM schemes when the approximate Roe matrix is computed using different types of numerical integration. In this regard, we conclude that there are almost no differences between the results obtained with each quadrature rule, whereas the midpoint rule (3.3) is much faster, essentially because multiplying by flux Jacobian matrices can be performed relatively faster by exploiting its structure.

Our last contribution stems from the fact that the characteristic fields are neither genuinely nonlinear nor linearly degenerate, so the maximal characteristic speed in a segment that joins two adjacent states may be attained in a point strictly in the interior of the segment. To prevent possible entropy violations we bound all characteristic velocities at points in the segment by using the bounds provided by the interlacing property.

With respect to the quality of the numerical solutions, the best first order numerical scheme is, of course Roe's method if we could calculate a Roe matrix followed by PVM-4, PVM-2 and HLL method. PVM-2 is an interesting choice, as it is an upwind scheme and provides results as good as PVM-2. To conclude the PVM schemes are an excellent alternative to Roe methods to approximate time-dependent solutions when computing the spectral information of the flux Jacobian is very expensive.

Acknowledgements

RB is supported by Fondecyt project 1130154; BASAL project CMM, Universidad de Chile and Centro de Investigación en Ingeniería Matemática (CI^{2}MA), Universidad de Concepción; Conicyt project Anillo ACT1118 (ANANUM); and CRHIAM, project CONICYT/FONDAP/15130015. In addition RB and LR are supported by Red Doctoral REDOC.CTA, MINEDUC project UCO1202. PM is supported by Spanish MINECO projects MTM2011-22741 and MTM2014-54388-P. LR is supported by Conicyt scholarship.

References

[1] P.L. Roe, Approximate Riemann solvers, parameter vectors and difference schemes, J Comput Phys 43 (1981), 357–371.

[2] C.E. Castro and E.F. Toro, Roe-type Riemann solvers for general hyperbolic systems, Int J Numer Meth Fluids 75 (2014), 467–486.

[3] R. Bürger, R. Donat, P. Mulet and C.A. Vega, Hyperbolicity analysis of polydisperse sedimentation models via a secular equation for the flux Jacobian, SIAM J Appl Math 70 (2010), 2186–2213.

[4] R. Donat and P. Mulet, Characteristic-based schemes for multi-class Lighthill-Whitham-Richards traffic models, J Sci Comput 37 (2008), 233–250.

[5] P. Degond, P.F. Peyrard, G. Russo and P. Villedieu, Polynomial upwind schemes for hyperbolic systems, C R Acad Sci Paris Sér I 328 (1999), 479–483.
[6] M.J. Castro Díaz and E. Fernández-Nieto, A class of computationally fast first order finite volume solvers: PVM methods, SIAM J Sci Comput 34 (2012), A2173–A2196.
[7] R. Bürger and A. Kozakevicius, Adaptive multiresolution WENO schemes for multi-species kinematic flow models, J Comput Phys 224 (2007), 1190–1222.
[8] M.J. Lighthill and G.B. Whitham, On kinematic waves: II. A theory of traffic flow on long crowded roads, Proc Royal Soc A 229 (1955), 317–345.
[9] P.I. Richards, Shock waves on the highway, Oper Res 4 (1956), 42–51.
[10] S. Benzoni-Gavage and R.M. Colombo, An n-populations model for traffic flow, Eur J Appl Math 14 (2003), 587–612.
[11] G.C.K. Wong and S.C. Wong, A multi-class traffic flow model: an extension of LWR model with heterogeneous drivers, Transp Res Part A 36 (2002), 827–841.
[12] F. Rosso and G. Sona, Gravity-driven separation of oilwater dispersions, Adv Math Sci Appl 11 (2001), 127–151.
[13] R. Bürger, R. Donat, P. Mulet and C.A. Vega, On the implementation of WENO schemes for a class of polydisperse sedimentation models, J Comput Phys 230 (2011), 2322–2344.
[14] J. Anderson, A secular equation for the eigenvalues of a diagonal matrix perturbation, Linear Algebra Appl 246 (1996), 49–70.
[15] R. Donat and P. Mulet, A secular equation for the Jacobian matrix of certain multi-species kinematic flow models, Numer Methods Partial Differential Equations 26 (2010), 159–175.
[16] M.J. Lockett and K.S. Bassoon, Sedimentation of binary particle mixtures, Powder Technol 24 (1979), 1–7.
[17] J.H. Masliyah, Hindered settling in a multiple-species particle system, Chem Engrg Sci 34 (1979), 1166–1168.
[18] R. Bürger, K.H. Karlsen, E.M. Tory and W.L. Wendland, Model equations and instability regions for the sedimentation of polydisperse suspensions of spheres, ZAMM Z Angew Math Mech 82 (2002), 699–722.
[19] J.F. Richardson and W.N. Zaki, Sedimentation and fluidization: Part I, Trans Instn Chem Engrs (London) 32 (1954), 35–53.
[20] B.D. Greenshields, A study of traffic capacity, Highway Research Board Proceedings 14 (1935), 448–477.
[21] J.S. Drake, J.L. Schofer and A.D. May, A statistical analysis of speed-density hypotheses, Highway Research Record 154 (1967), 53–87.
[22] P. Zhang, R.-X. Liu, S.C. Wong and S.-Q. Dai, Hyperbolicity and kinematic waves of a class of multipopulation partial differential equations, Eur J Appl Math 17 (2006), 171–200.
[23] A. Harten, P.D. Lax and B. van Leer, On upstream differencing and Godunov type schemes for hyperbolic conservation laws, SIAM Rev 25 (1983), 35–61.
[24] B. van Leer, Towards the ultimate conservative finite difference scheme, V. A second order sequel to Godunov's method, J Comput Phys 32 (1979), 101–136.
[25] W. Schneider, G. Anestis and U. Schaflinger, Sediment composition due to settling of particles of different sizes, Int J Multiphase Flow 11 (1985), 419–423.
[26] P.T. Shannon, E. Stroupe and E.M. Tory, Batch and continuous thickening, Ind Eng Chem Fund 2 (1963), 203–211.
[27] M. Zhang, C.-W. Shu, G.C.K. Wong and S.C. Wong, A weighted essentially non-oscillatory numerical scheme for a multi-class Lighthill-Whitham-Richards traffic flow model, J Comput Phys 191 (2003), 639–659.

Centro de Investigación en Ingeniería Matemática (CI^{2}MA)

PRE-PUBLICACIONES 2015

2015-18 Anahi Gajardo, Diego Maldonado, Andres Moreira: *Universal time-symmetric number-conserving cellular automaton.*

2015-19 Johnny Guzman, Filander A. Sequeira, Chi - Wang Shu: *H(div) conforming and DG methods for the incompressible Euler equations*

2015-20 Raimund Bürger, Stefan Diehl, Camilo Mejías: *On time discretizations for the simulation of the settling-compression process in one dimension*

2015-21 Veronica Anaya, David Mora, Ricardo Ruiz-Baier: *Pure vorticity formulation and Galerkin discretization for the Brinkman equations*

2015-22 Ana Alonso-Rodriguez, Jessika Camaño, Riccardo Ghiloni, Alberto Valli: *Graphs, spanning trees and divergence-free finite elements in general topological domains*

2015-23 Gabriel N. Gatica, Filander A. Sequeira: *Analysis of the HDG method for the Stokes-Darcy coupling*

2015-24 Marco Discacciati, Ricardo Oyarzúa: *A conforming mixed finite element method for the Navier-Stokes/Darcy coupled problem*

2015-25 Julio Aracena, Adrien Richard, Lilian Salinas: *Fixed points in conjunctive networks and maximal independent sets in graph contractions*

2015-26 Margareth Alves, Jaime Muñoz-Rivera, Mauricio Sepúlveda: *Exponential stability to Timoshenko system with shear boundary dissipation*

2015-27 Ricardo Oyarzúa, Paulo Zuñiga: *Analysis of a conforming finite element method for the Boussinesq problem with temperature-dependent parameters*

2015-28 Fernando Betancourt, Fernando Concha, Lina Uribe: *Settling velocities of particulate systems part 17. Settling velocities of individual spherical particles in power-law non-Newtonian fluids*

2015-29 Raimund Bürger, Pep Mulet, Lihki Rubio: *Polynomial viscosity methods for multispecies kinematic flow models*

Para obtener copias de las Pre-Publicaciones, escribir o llamar a: Director, Centro de Investigación en Ingeniería Matemática, Universidad de Concepción, Casilla 160-C, Concepción, Chile, Tel.: 41-2661324, o bien, visitar la página web del centro: `http://www.ci2ma.udec.cl`







Centro de Investigación en
Ingeniería Matemática (CI²MA)
Universidad de Concepción

Casilla 160-C, Concepción, Chile
Tel.: 56-41-2661324/2661554/2661316
http://www.ci2ma.udec.cl